IET Microwaves, Antennas & Propagation

Special Issue: Microwave Components and Antennas Based on Advanced Manufacturing Techniques

Additively manufactured artificial materials with metallic meta-atoms

ISSN 1751-8725
Received on 31st October 2016
Revised 18th July 2017
Accepted on 25th July 2017
E-First on 5th October 2017
doi: 10.1049/iet-map.2016.0952
www.ietdl.org

Shiyu Zhang[1] ✉, William Whittow[1], John (Yiannis) C. Vardaxoglou[1]

[1]*Wolfson School of Mechanical, Electrical and Manufacturing Engineering, Loughborough University, Leicestershire, Loughborough LE11 3TU, UK*

✉ *E-mail: S.Zhang@lboro.ac.uk*

Abstract: This study presents the analysis and fabrication of artificial materials with metallic cuboid inclusions (termed here as meta-atoms) in a dielectric host material. These synthetic materials or metamaterials have been additively manufactured with a fused deposition modelling three-dimensional (3D) printer. The effective permittivity and permeability have been numerically analysed using the Maxwell–Garnett and Lewin's approximation. Simulations and measurements have shown good agreement with analytical calculations. The anisotropy of the heterogeneous mixture due to the orientation of the meta-atoms has been demonstrated. The effective permittivity has been increased by the presence of the meta-atoms, which has the potential of producing 3D-printing metamaterials with tailored electromagnetic properties.

1 Introduction

Metamaterials have distinct electromagnetic (EM) properties and have advantages in numerous applications such as antennas, lenses, acoustics and cloaking [1–3]. These new materials can tailor the EM properties and hence control the EM wave propagation. They can be used to design new antenna substrates or superstrates that have fabricational, physical and EM advantages over conventional dielectric materials. There are many research papers that have discussed artificial materials and metamaterials with tailored EM properties [4–9]. Artificial heterogeneous materials can be constructed by adding metallic inclusions arranged in different lattices and this can control the effective EM properties including permittivity, permeability and losses [10–14]. Hence engineers in principle can design radio-frequency (RF) materials with bespoke EM properties and thicknesses by changing the inclusions (meta-atoms) and their volume fraction.

These so-called 'meta-atoms' can be defined as inclusions whose size is much smaller than the wavelength of operation and have arbitrary constitutive parameters arranged in regular or irregular lattices. Metallic meta-atoms can increase the effective relative permittivity ($\varepsilon_{\text{reff}}$) of the structure. These inclusions however give rise to diamagnetism where the effective relative permeability (μ_{reff}) of the substrate is smaller than 1. In general, the $\varepsilon_{\text{reff}}$ and μ_{reff} depend on the volume fraction of the inclusion and host materials. Furthermore, the shapes of the metallic inclusions may result in anisotropy. The anisotropic and diamagnetic effects due to cuboid metallic inclusions have been analysed using EM simulations in [15, 16], but fabrications of such heterogeneous material have not been widely reported in the literature. The artificial anisotropic dielectrics will give extra design freedom for future innovative antenna applications. A dielectric anisotropic substrate for generating circular polarisation has been reported in [17]. The metallic meta-atom-based heterogeneous material has the potential of providing a wider range of controlling the anisotropy and the EM field.

Manufacturing metamaterials with metallic inclusions is cumbersome. It usually involves several processes such as micromachining, etching and assembling [18–20]. A simple manufacturing technique is highly desirable. Advanced digital additive manufacturing (AM) technology builds a three-dimensional (3D) object in successive layers. This fabrication process has less material waste, and gives extra freedom for designing bespoke EM materials, which may be particularly useful for high value, but low volume products. Several antennas and RF components such as lenses, frequency selective surface and waveguides have been be fabricated by AM which are more economical and provide extra design freedom compared with conventional techniques [21–26]. Furthermore, as there was no machining or bonding, this manufacturing technique enhanced the physical durability of the materials. Isakov *et. al.* [27] have used 3D printing to fabricate anisotropic fully dielectric media. 3D-printed dielectrics and metals combined together in a layered fashion for artificial materials or metamaterial fabrication have not been reported in the literature.

This paper proposes a practicable procedure for designing and fabricating metamaterials with both dielectric and metallic inclusions. AM was used for fabricating the dielectric layers with empty cuboids which were then filled with conductive paste. This allowed the deposition of the metallic inclusions (meta-atoms) inside each dielectric layer during the fabrication process. The detailed manufacturing process is presented in Section 2.

Section 3 presents the principle formulations for estimating the effective permittivity and permeability of a heterogeneous material with metallic cuboids. The analytically calculated results are compared with full wave simulations and measurements in Section 4. The results have shown the anisotropic and diamagnetic ($\mu_{\text{reff}} < 1$) effects. The meta-atoms resulted in an increased $\varepsilon_{\text{reff}}$ of the synthetic mixtures.

In Section 5, the effects of the distance between meta-atoms has been examined. Metamaterials with different distances between the meta-atoms have been fabricated and measured to show the effects on the EM properties of the metallic inclusions. The conclusions are summarised in Section 6.

2 Additively fabricated metamaterial samples

A fused deposition modelling 3D printer (Makerbot Replicator 2X) was used to fabricate the dielectric layers of the metamaterial structures. The sketch of the printed metamaterial with meta-atoms is shown in Fig. 1. The 3D models were designed using computer-aided design (CAD) tools and were subsequently sliced into successive layers by the software. The heated printer nozzle extruded the thermal 3D-printing material and created the host structure layer by layer from the bottom upwards. Thermoplastic polyester polylactic acid (PLA) was used as the 3D-printing material. The extrusion temperature of the printer nozzle for PLA

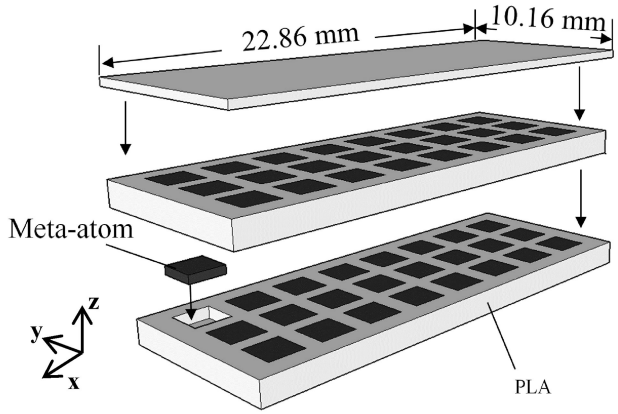

Fig. 1 *Sketch of 3D-printed metamaterial sample with two layers of meta-atoms*

was 200°C. The conductivity of the silver paste was measured as 5.7×10^5 S/m by using the van der Pauw method [28].

First, an 'ice cube tray' type host structure was printed, as shown in Fig. 2*a*. There were a number of empty blocks in the 'ice cube tray' for hosting the meta-atoms. In this work, the size of the meta-atom was kept constant and the dimensions of the empty block were $1.3 \times 1.3 \times 0.3$ mm^3. After the 'ice cube tray' was finished, the print job was paused and conductive silver paste was filled into the empty blocks manually using a syringe without moving the host, as shown in Fig. 2*b*. After all the cuboids were filled, the print was resumed and the second layer of PLA host was printed directly on top of the first one. Then, the second layer of meta-atoms was added by filling the paste into the empty blocks. Finally, a PLA lid was printed on top. The PLA host layers did not move during the whole fabrication process to ensure the host layers and the meta-atoms were aligned. Fig. 2*c* shows the photograph of the finished sample.

3 Numerical approach for calculating effective EM properties

The cuboid shape of the meta-atom caused a non-uniform disturbance of the electric and magnetic fields. Therefore, the $\varepsilon_{\text{reff}}$ and μ_{reff} of the mixture are different according to the orientation of the meta-atoms. The effective dielectric permittivity of a periodic composite materials can be determined by using the Maxwell–Garnett formula [29]. The formula was further modified to solve various inclusion shapes including ellipsoids. The depolarisation factor N_j ($j = a, b, c$) of in the axes of an ellipsoid inclusion with three semi-axes a, b and c is defined in [30]

$$N_j = \frac{abc}{2}\int_0^\infty \frac{\mathrm{d}u}{(j^2+u)\sqrt{(a^2+u)(b^2+u)(c^2+u)}} \tag{1}$$

Since both ellipsoids and cuboids have three major axes that determine their 3D shapes, here the ellipsoid model is used to approximate the cuboid inclusions. Assuming the ellipsoid and cuboid inclusions have the same aspect ratio, the depolarisation factor N_j in the axes of a cuboid inclusion with three semi-axes a, b and c can be also obtained using (1), where j is one of the semi-axes of the cuboid. Thus, the depolarisation factor N_a has $j = a$, N_b has $j = b$ and N_c has $j = c$, and they satisfy the following relationship, $N_a + N_b + N_c = 1$.

Then if the incident electric field is parallel to one of the cuboid edges, the modified Maxwell–Garnett formula for ellipsoid inclusions [30] can be used to approximate the cuboid inclusions

$$\varepsilon_{\text{eff},\,j} = \varepsilon_h + f\varepsilon_h \frac{\varepsilon_i - \varepsilon_h}{\varepsilon_h + (1-f)N_j(\varepsilon_i - \varepsilon_h)} \tag{2}$$

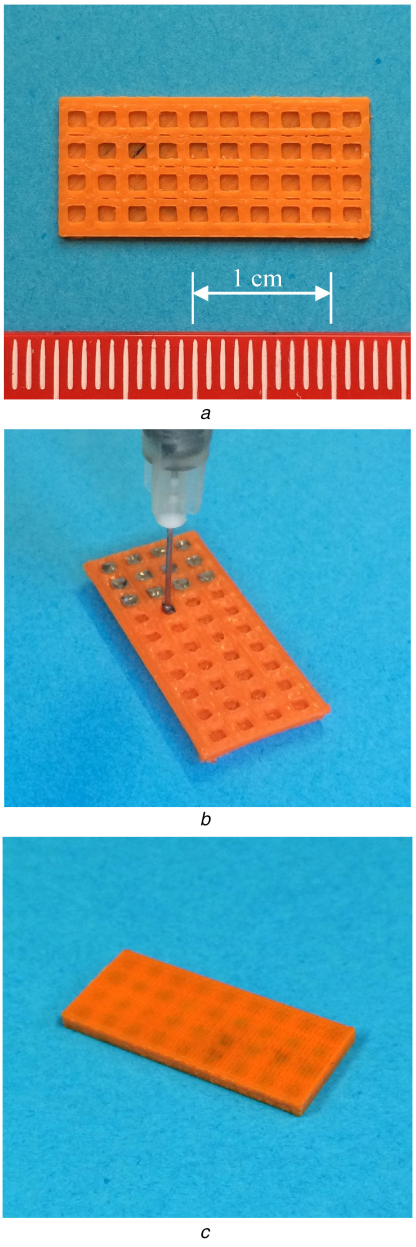

Fig. 2 *Fabrication process of metamaterial sample*
(a) 3D-printed PLA dielectric layer (host structure, the 'ice cube tray'), ***(b)*** Filling conductive silver paste to form the meta-atoms, ***(c)*** Finished sample

where the $\varepsilon_{\text{eff},\,j}$ is the effective permittivity of the mixture for the j-component, ε_h and ε_i are the permittivities of the host and inclusion, respectively, f is the volume fraction of the inclusions.

Similarly, the effective permeability of the mixture for the H-field that is parallel to j-edge is

$$\mu_{\text{eff},\,j} = \mu_h + f\mu_h \frac{\mu_i - \mu_h}{\mu_h + (1-f)N_j(\mu_i - \mu_h)} \tag{3}$$

where the μ_h and μ_i are the permeabilities of the host and inclusion, respectively.

It is worth noting that the depolarisation factor N_j should be calculated for the electric field and magnetic field separately, as the directions of the electric field or magnetic field relative to edges of inclusion are different.

The ε_i and μ_i in (2) and (3) are the properties of the bulk material. However, the bulk material EM properties cannot be used to represent small inclusions, typically $\ll \lambda/10$. Lewin [31] defined that a small inclusion with very small physical size would have the 'effective permittivity and permeability of the particle' that are relative to its total external field including the scattered field due to

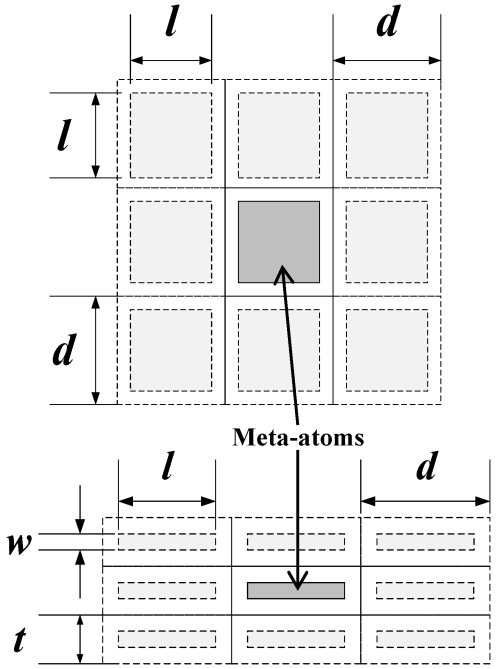

Fig. 3 *2D view of the unit cells with meta-atoms in a lattice*

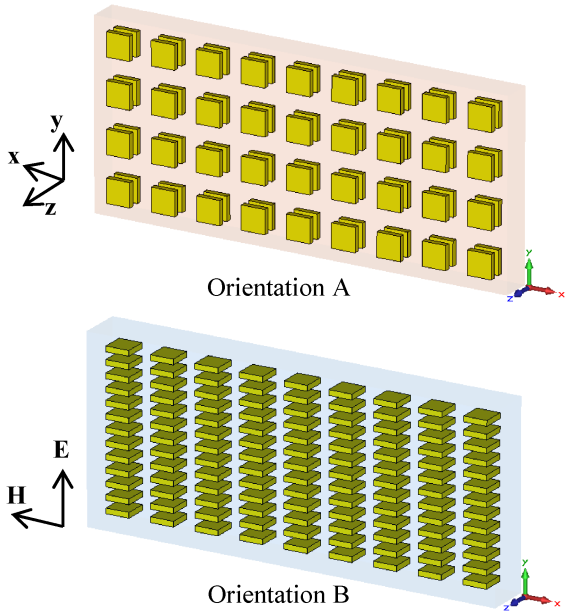

Fig. 4 *Sketches of waveguide-sized samples with two orientations of meta-atoms*

that inclusion. In this paper, in order not to confuse with the effective permittivity and permeability of the mixture, here we use the 'apparent permittivity and permeability' of the inclusions $\varepsilon_{a,i}$ and $\mu_{a,i}$ to indicate the effective permittivity and permeability of the particle. The $\varepsilon_{a,i}$ and $\mu_{a,i}$ can be modified from the bulk properties of the inclusion [31]

$$\frac{\varepsilon_{a,i}}{\varepsilon_i} = \frac{\mu_{a,i}}{\mu_i} = \frac{2(\sin\theta - \theta\cos\theta)}{(\theta^2 - 1)\sin\theta + \theta\cos\theta} = F(\theta) \tag{4}$$

where $\theta = (2\pi a\sqrt{\varepsilon_i\mu_i})/\lambda$, $k = 2\pi/\lambda$. Lewin only discussed spherical inclusions in [31] and a is the radius of the particle. In our case, a is replaced by the half length of the edge that is parallel to the electric field.

Now, (2) and (3) can be re-written as the new expressions

$$\varepsilon_{\text{eff},j} = \varepsilon_h + f\varepsilon_h \frac{\varepsilon_{a,i} - \varepsilon_h}{\varepsilon_h + (1-f)N_j(\varepsilon_{a,i} - \varepsilon_h)} \tag{5}$$

$$\mu_{\text{eff},j} = \mu_h + f\mu_h \frac{\mu_{a,i} - \mu_h}{\mu_h + (1-f)N_j(\mu_{a,i} - \mu_h)} \tag{6}$$

Equations (5) and (6) can be used to solve general two-material mixing problems for cuboid inclusions.

Metallic inclusions generally have a very large ε_i due to the high conductivity. This results in θ being large and complex which leads to $\varepsilon_{a,i} \gg \varepsilon_h$. Therefore, (5) can be simplified as in (7)

$$\varepsilon_{\text{eff},j} = \varepsilon_h + f\frac{\varepsilon_h}{(1-f)N_j} \tag{7}$$

We assume that both the inclusions and the host materials are non-magnetic, $\mu_h = \mu_i = 1$. However, it has $\mu_{a,i} \to 0$ according to (4). So, the expression of $\mu_{\text{eff},j}$ for metallic inclusions can be simplified as

$$\mu_{\text{eff},j} = \mu_h + f\frac{\mu_h}{(1-f)N_j - 1} \tag{8}$$

Equations (7) and (8) will be used for estimating effective permittivity and permeability of the 3D-printed samples in Sections 4 and 5.

4 Evaluation of anisotropy and diamagnetism

Two orientations were simulated and measured in this section, as shown in Fig. 3. The meta-atom was situated in the centre of the host material to form a unit cell. Fig. 3 shows 2D views of the unit cells with the meta-atoms in a lattice. It is critical to avoid current flowing between the meta-atoms that would occur if they touched. In this work, all the meta-atoms were the same size with $l = 1.3$, $w = 0.3$, $d = 2.5$ and $t = 0.85$ mm.

The fabricated samples were simulated by using CST and measured over the X-band frequency range. The samples were fabricated to fit exactly in a rectangular WR90 waveguide (22.86×10.16 mm^2). The Nicolson–Ross and Weir (NRW) method [32, 33] was used to retrieve the effective EM properties of the samples for both simulations and measurements. The sketches of two waveguide-sized samples are shown in Fig. 4. For simplicity, only two layers in the z-axis of meta-atoms were applied for orientation A. Owing to the NRW restriction on the sample thickness ($< \lambda_g/4$), only one unit cell of meta-atoms in the z-axis was applied for orientation B.

Fig. 5 shows the photographs of the fabricated samples. Orientation A was fabricated as the description in Section 2. It had two layers in the z-axis. Orientation B was printed with multiple PLA host layers stacked up in the y-axis. Although orientation B could also be built up in the z-axis direction, the empty blocks for the meta-atoms could not be printed properly due to their narrow thicknesses w. A 3D printer with higher resolution and a finer nozzle would address this problem. Since orientation B required more pauses in the printing process and more manual deposition of silver paste, the physical imperfections of orientation B were higher due to spilled-over silver paste and miss-aligned cuboids. This can be seen in Fig. 5. The dimensions of the CAD model of orientation A were $22.86 \times 10.16 \times 1.70$ mm^3 and the dimensions of the fabricated sample as measured by a caliper were $22.76 \times 10.16 \times 1.73$ mm^3. The CAD model and the fabricated sample dimensions of orientation B were $22.86 \times 10.16 \times 2.50$ and $22.81 \times 10.15 \times 2.51$ mm^3, respectively.

EM simulations were carried out to verify the measurement. The simulations were designed to replicate the real measurement setup: the metamaterial samples were modelled using the measured outer dimensions and were placed in a WR90 waveguide; the dielectric constant of the host PLA was 2.69 and electric loss tangent was 0.01 as taken from waveguide measurement at 10 GHz. The conductivity of the meta-atoms was used as the value of the silver paste (5.7×10^5 S/m).

The retrieved results from the simulations are shown in Table 1, and compared with measured results and the results that were

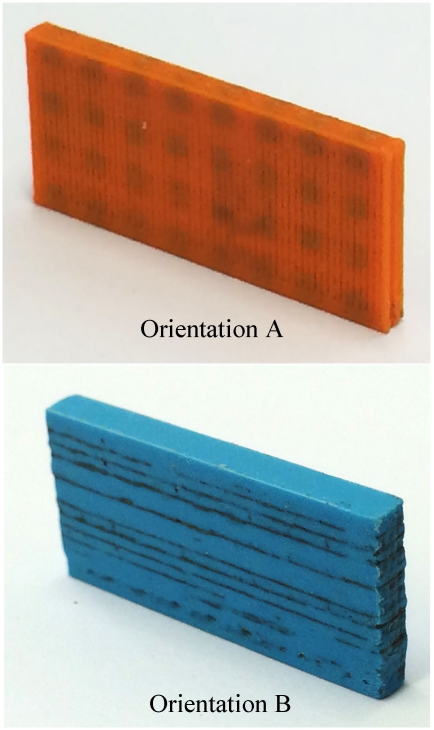

Fig. 5 *Photographs of additively manufactured metamaterial samples*

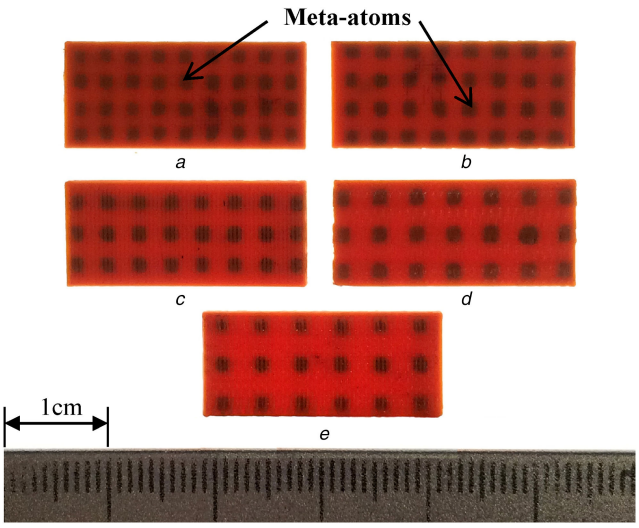

Fig. 6 *3D-printed artificial dielectrics samples with different periodicities of metallic inclusions*
(a) $d = 2.50$ mm, ***(b)*** $d = 2.75$ mm, ***(c)*** $d = 3.00$ mm, ***(d)*** $d = 3.50$ mm, ***(e)*** $d = 3.75$ mm

calculated using (7) and (8). Table 1 shows the diamagnetic effect with $\mu_{reff} < 1$ due to the embedded meta-atoms. The ε_{reff} of the mixtures were all higher than the host PLA. Although (7) and (8) cannot evaluate the losses, they can still be used for predicting the ε_{reff} and μ_{reff} for the different meta-atom orientations. Note the calculation used ellipsoids to approximate the cuboids and there are differences between the calculations and the full wave simulations.

The measured ε_{reff} of orientation A was higher than orientation B, which agreed well with the simulations and analytical calculations. Note orientation A contained a lower volume of metal (72 meta-atoms embedded), compared with B (117 meta-atoms). This indicates that the orientation of the anisotropic metallic inclusions has a more significant effect on the ε_{reff} compared with the volume fraction. The meta-atoms had its maximum effect when the largest surface was parallel to the electric field. Both orientations had their largest surface parallel to the magnetic field, and therefore the μ_{reff} for both orientations were similar – see Table 1.

5 Effect of distance between meta-atoms

With the size of the meta-atom was fixed, by varying the distance d, different volume fractions of the meta-atoms were achieved. As described in Section 4, fabricating orientation B resulted in a greater number of manual processes. Therefore, only samples with orientation A were compared in this section. Five samples with different d values were fabricated: 2.50, 2.75, 3.00, 3.50 and 3.75 mm. Note, smaller d values resulted in more meta-atoms in the metamaterial samples. Fig. 6 shows the photographs of all the five samples. A bright light was placed underneath of the samples to illuminate the embedded meta-atoms which can be observed as the dark squares seen through the PLA cover. As shown, sample $d = 2.50$ mm had the most cuboids in each layer ($9 \times 4 = 36$), whereas 3.75 mm sample had the fewest ($6 \times 3 = 18$). The ε_{reff} of the samples was analytically calculated to be between 3.56 and 4.62, and the μ_{reff} was calculated to be between 0.90 and 0.95 by using (7) and (8), respectively.

Fig. 7 shows the measured ε_{reff} of the metamaterial samples. The host material PLA had $\varepsilon_{reff} = 2.69$ measured at 10 GHz. It can be seen that all the metamaterials had higher ε_{reff} than the host PLA. The ε_{reff} was stable across the frequency range and agreed well with simulated results. The ε_{reff} was higher when the meta-atoms were closer. The highest ε_{reff} was 4.50 at 10 GHz with $d = 2.50$ mm. The μ_{reff} decreased with reduced spacing between the meta-atoms, see Fig. 8. All the metamaterial samples have $\mu_{reff} < 1$. The lowest μ_{reff} at 10 GHz was obtained as 0.88 with the $d = 2.50$ mm sample. Although the ε_{reff} increased and the μ_{reff} decreased with the reduced distance d, the effective refractive index of the samples was increased. In simulations, the samples had six smooth surfaces, but the printed samples had rough surfaces (see Fig. 6) due to the AM process. The surface roughness of the printed samples resulted in the differences between the simulated and measured results. The calculated ε_{reff} and μ_{reff} using (7) and (8) are shown in Figs. 7*b* and 8*b*, respectively. Since (7) and (8) are frequency independent, the calculated results are shown at 10 GHz. The calculated results show reasonable agreement with the simulations and measurements.

Figs. 9 and 10 show the effective electric loss tangent and magnetic loss tangent, respectively. The real (ε'_{reff}, μ'_{reff}) and imaginary (ε''_{reff}, μ''_{reff}) parts of the effective relative permittivity and permeability were retrieved using the NRW method. Then, the electric and magnetic loss tangent values were calculated using $\tan\delta_e = \varepsilon''_{reff}/\varepsilon'_{reff}$ and $\tan\delta_m = \mu''_{reff}/\mu'_{reff}$, respectively. Fig. 9 indicates that both the electric and magnetic losses were increased with the closer meta-atoms, which agrees with the simulated results in Fig. 10. The lowest $\tan\delta_e$ averaged over the frequency range was 0.010 with $d = 3.75$ mm, whereas the highest average $\tan\delta_e$ was 0.017 with $d = 2.50$ mm. The lowest and highest average $\tan\delta_m$ were 0.009 and 0.028.

Table 1 Comparison of effective EM properties of metamaterial samples with meta-atoms in different orientations

	Orientation A				Orientation B			
Number of meta-atoms	72				117			
Effective EM properties	ε_r	$\tan\delta_e$	μ_r	$\tan\delta_m$	ε_r	$\tan\delta_e$	μ_r	$\tan\delta_m$
calculated	4.62	—	0.90	—	3.11	—	0.88	—
simulated	4.57	0.017	0.91	0.015	3.40	0.010	0.86	0.004
measured	4.53	0.017	0.88	0.003	3.28	0.002	0.91	0.002

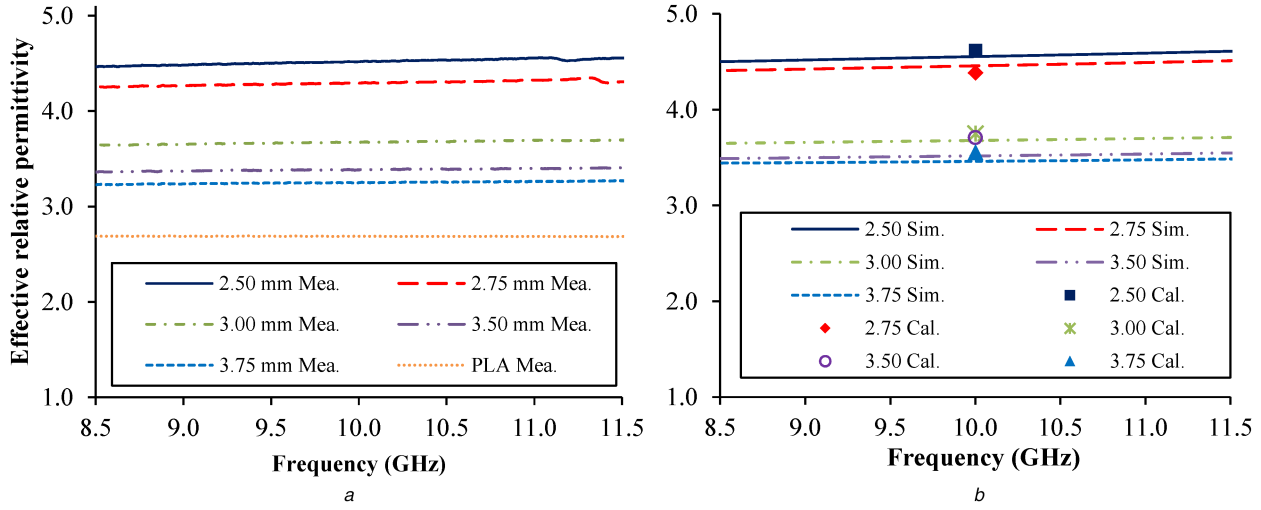

Fig. 7 *Effective relative permittivity of metamaterial samples*
(a) Measured ε_{reff}, ***(b)*** Simulated ε_{reff} and calculated ε_{reff} using (7)

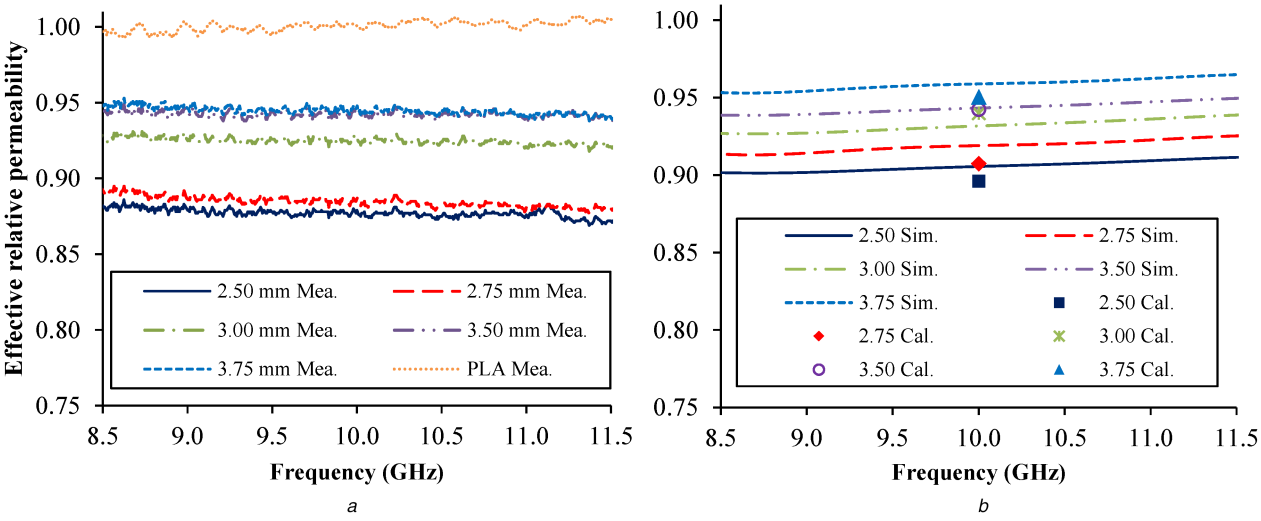

Fig. 8 *Effective relative permeability of metamaterial samples*
(a) Measured μ_{reff}, ***(b)*** simulated μ_{reff} and calculated μ_{reff} using Equation (8)

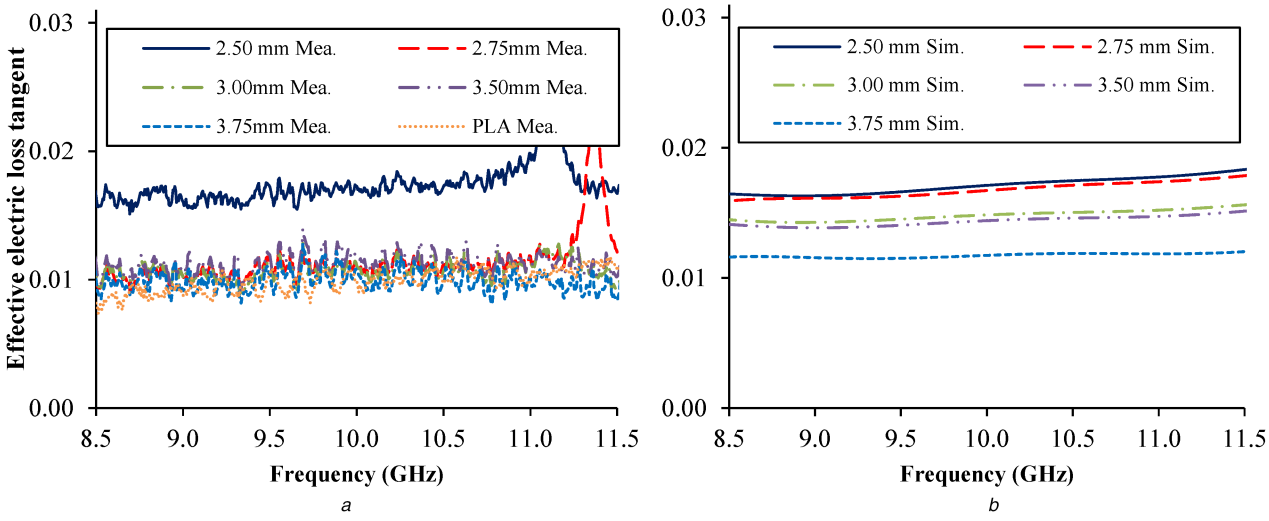

Fig. 9 *Effective electric loss tangent*
(a) Measured tan δ_e, ***(b)*** Simulated tan δ_e

6 Conclusions and discussion

Metamaterials with regular metallic meta-atoms have been successfully fabricated and measured. In general, these metallic cuboid inclusions placed in an array to form an artificial dielectric increased the effective relative permittivity compared with the host material. The measured results agreed well with the numerical calculations and full wave simulations. This indicated that metamaterials with tailored EM properties can be fabricated by controlling the distribution of the inclusions. The numerical

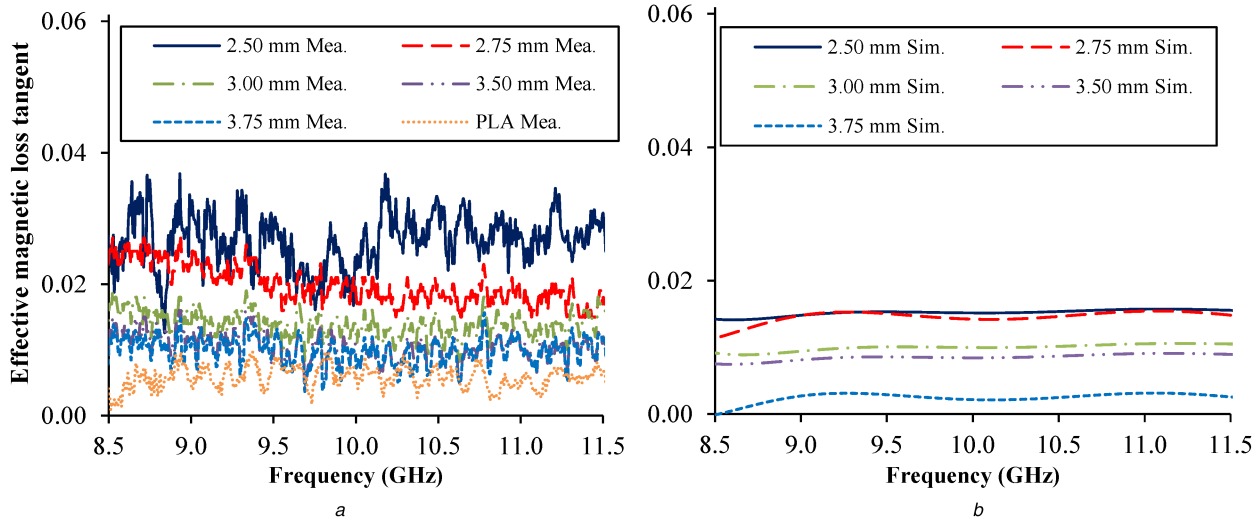

Fig. 10 *Effective magnetic loss tangent*
(a) Measured tan δ_m, ***(b)*** Simulated tan δ_m

analysis can be initially used to assist the design. The anisotropic effects have been examined and depend on the orientation of the metallic cuboids. Anisotropic metallic cuboid inclusions with their largest surface parallel to the electric field resulted in the most significant increase in the effective relative permittivity. The orientation was more significant than the volume fraction of the metallic inclusions. The effective relative permittivity was larger with the closer metallic cuboids (higher volume fraction of inclusions). Measurements have shown that diamagnetic effects were introduced with the metallic inclusions. The closer metallic inclusion also increased electric and magnetic losses.

The AM technique can effectively fabricate heterogeneous metamaterials with bespoke internal structures that are difficult to produce by traditional micromachining. Although there were imperfections in the fabricated samples, this work has successfully demonstrated using the conductive paste to form metallic inclusions, and the measured results reasonably agreed with the simulations. Therefore, a modified 3D printer with two nozzles that provides both polymer and conductive paste extrusion can address the challenge of fabricating the metamaterials in a single process. Furthermore, higher-precision facilities are desirable for fabricating the small-scale elements which are critical to higher frequencies such as millimetre wave and terahertz applications.

7 Acknowledgments

This work was supported by the EPSRC research grant SYMETA (EP/N010493/1) and the EPSRC Doctoral Prize Research Fellowship.

8 References

[1] Ziolkowski, R.W., Erentok, A.: 'Metamaterial-based efficient electrically small antennas', *IEEE Trans. Antennas Propag.*, 2006, **54**, (7), pp. 2113–2130
[2] Jiang, W.X., Cui, T.J., Ma, H.F., *et al.*: 'Layered high-gain lens antennas via discrete optical transformation', *Appl. Phys. Lett.*, 2008, **93**, (22), p. 221906
[3] Schurig, D., Mock, J.J., Justice, B.J., *et al.*: 'Metamaterial electromagnetic cloak at microwave frequencies', *Science (New York, NY)*, 2006, **314**, (5801), pp. 977–980
[4] Zhang, Y., Mittra, R., Hong, W.: 'On the synthesis of a flat lens using a wideband low-reflection gradient-index metamaterial', *J. Electromagn. Waves Appl.*, 2011, **25**, (16), pp. 2178–2187
[5] Njoku, C.C., Whittow, W.G., Vardaxoglou, J.C.: 'Simulation methodology for synthesis of antenna substrates with microscale inclusions', *IEEE Trans. Antennas Propag.*, 2012, **60**, (5), pp. 2194–2202
[6] Zhang, Y., Mittra, R., Hong, W.: 'Systematic design of planar lenses using artificial dielectrics'. 2010 IEEE Int. Symp. Antennas and Propagation and CNC-USNC/URSI Radio Science Meeting – Leading the Wave, 2010, AP-S/URSI 2010
[7] Chen, X., Feng Ma, H., Ying Zou, X., *et al.*: 'Three-dimensional broadband and high-directivity lens antenna made of metamaterials', *J. Appl. Phys.*, 2011, **110**, (4), p. 44904
[8] Njoku, C.C., Whittow, W.G., Vardaxoglou, J.C.: 'Comparative study of nanomaterials' effective properties using canonical formations'. Antennas and Propagation Conf. (LAPC), 2010, Loughborough, 2010
[9] Smith, D.R., Schurig, D., Rosenbluth, M., *et al.*: 'Limitations on subdiffraction imaging with a negative refractive index slab', *Appl. Phys. Lett.*, 2003, **82**, (10), pp. 1506–1508
[10] Cai, X., Zhu, R., Hu, G.: 'Experimental study for metamaterials based on dielectric resonators and wire frame', *Metamaterials*, 2008, **2**, (4), pp. 220–226
[11] Holloway, C.L., Kuester, E.F., Baker-Jarvis, J., *et al.*: 'A double negative (DNG) composite medium composed of magnetodielectric spherical particles embedded in a matrix', *IEEE Trans. Antennas Propag.*, 2003, **51**, (10), pp. 2596–2603
[12] Lord Rayleigh: 'LVI. on the influence of obstacles arranged in rectangular order upon the properties of a medium', *Philos. Mag. Ser. 5*, 1892, **34**, (211), pp. 481–502
[13] Brown, J.: 'Artificial dielectrics having refractive indices less than unity', *Proc. IEE IV, Inst. Monogr.*, 1953, **100**, (5), pp. 51–62
[14] Doyle, W.T.: 'Optical properties of a suspension of metal spheres', *Phys. Rev. B*, 1989, **39**, (14), pp. 9852–9858
[15] Njoku, C.C., Whittow, W.G., Vardaxoglou, J.C.: 'Microstrip patch antennas with anisotropic and diamagnetic synthetic heterogeneous substrates', *IEEE Trans. Antennas Propag.*, 2015, **63**, (7), pp. 3280–3285
[16] Wu, W.M., Njoku, C.C., Whittow, W.G., *et al.*: 'Studies of permittivity and permeability of dielectric matrix with cuboid metallic inclusions in different orientations', *J. Adv. Dielectr.*, 2014, **4**, (4), p. 1450032
[17] Tuovinen, T., Salonen, E.T., Berg, M.: 'An artificially anisotropic antenna substrate for the generation of circular polarization', *IEEE Trans. Antennas Propag.*, 2016, **64**, (11), pp. 4937–4942
[18] Parke, L., Hooper, I.R., Edwards, E., *et al.*: 'Independently controlling permittivity and diamagnetism in broadband, low-loss, isotropic metamaterials at microwave frequencies', *Appl. Phys. Lett.*, 2015, **106**, (10), p. 101908
[19] Ziolkowski, R.W.: 'Design, fabrication, and testing of double negative metamaterials', *IEEE Trans. Antennas Propag.*, 2003, **51**, (7), pp. 1516–1529
[20] Walia, S., Shah, C.M., Gutruf, P., *et al.*: 'Flexible metasurfaces and metamaterials: a review of materials and fabrication processes at micro- and nano-scales', *Appl. Phys. Rev.*, 2015, **2**, (1), p. 11303
[21] Le Sage, G.P.: '3D printed waveguide slot array antennas', *IEEE Access*, 2016, **4**, pp. 1258–1265
[22] Van Der Vorst, M., Gumpinger, J.: 'Applicability of 3D printing techniques for compact Ku-band medium/high-Gain antennas'. Tenth European Conf. Antennas and Propagation (EuCAP), Davos, 2016, pp. 1–4
[23] Sanz-Izquierdo, B., Parker, E.A.: '3-D printing of elements in frequency selective arrays', *IEEE Trans. Antennas Propag.*, 2014, **62**, (12), pp. 6060–6066
[24] Liang, M., Ng, W., Chang, K., *et al.*: 'A 3-D luneburg lens antenna fabricated by polymer jetting rapid prototyping', *IEEE Trans. Antennas Propag.*, 2014, **62**, (4), pp. 1799–1807
[25] Zhang, S.: 'Design and fabrication of 3D-printed planar Fresnel zone plate lens', *Electron. Lett.*, 2016, **52**, (10), pp. 833–835
[26] Zhang, B., Zirath, H.: 'Metallic 3-D printed rectangular waveguides for millimeter-wave applications', *IEEE Trans. Compon. Packag. Manuf. Technol.*, 2016, **6**, (5), pp. 796–804
[27] Isakov, D.V., Lei, Q., Castles, F., *et al.*: '3D printed anisotropic dielectric composite with meta-material features', *Mater. Des.*, 2016, **93**, pp. 423–430
[28] van der Pauw, L.J.: 'A method of measuring the resistivity and hall coefficient of discs of arbitrary shape', *Philips Res. Rep.*, 1958, **13**, (1), pp. 1–9
[29] Garnett, J.C.M.: 'Colours in metal glasses, in metallic films, and in metallic solutions. II', *Philos. Trans. R. Soc. A, Math. Phys. Eng. Sci.*, 1906, **205**, (387–401), pp. 237–288
[30] Sihvola, A.: '*Electromagnetic mixing formulas and applications*' (IET, London, 1999)
[31] Lewin, L.: 'The electrical constants of a material loaded with spherical particles', *J. Inst. Electr. Eng. III, Radio Commun. Eng.*, 1947, **94**, (27), pp. 65–68

[32] Nicolson, A.M., Ross, G.F.: 'Measurement of the intrinsic properties of materials by time-domain techniques', *IEEE Trans. Instrum. Meas.*, 1970, **19**, (4), pp. 377–382

[33] Weir, W.B.: 'Automatic measurement of complex dielectric constant and permeability at microwave frequencies', *Proc. IEEE*, 1974, **62**, (1), pp. 33–36